# Requirement of the nicotinic acetylcholine receptor $\beta 2$ subunit for the anatomical and functional development of the visual system

**Francesco Mattia Rossi*, Tommaso Pizzorusso†, Vittorio Porciatti‡, Lisa M. Marubio*§, Lamberto Maffei†‡, and Jean-Pierre Changeux*¶**

*Laboratoire de Neurobiologie Moléculaire, Centre National de la Recherche Scientifique, Unité de Recherche Associée 2182, Récepteurs et Cognition, Institut Pasteur, 28 Rue du Dr. Roux, 75724 Paris Cédex 15, France; †Scuola Normale Superiore, Piazza Cavalieri, 7-56100, Pisa, Italy; and ‡Istituto di Neurofisiologia Consiglio Nazionale delle Ricerche, Area della Ricerca San Cataldo, Via Moruzzi, 1-56100, Pisa, Italy

Contributed by Jean-Pierre Changeux, March 12, 2001

**In the mammalian visual system the formation of eye-specific layers at the thalamic level depends on retinal waves of spontaneous activity, which rely on nicotinic acetylcholine receptor activation. We found that in mutant mice lacking the $\beta 2$ subunit of the neuronal nicotinic receptor, but not in mice lacking the $\alpha 4$ subunit, retinofugal projections do not segregate into eye-specific areas, both in the dorso-lateral geniculate nucleus and in the superior colliculus. Moreover, $\beta 2-/-$ mice show an expansion of the binocular subfield of the primary visual cortex and a decrease in visual acuity at the cortical level but not in the retina. We conclude that the $\beta 2$ subunit of the nicotinic acetylcholine receptor is necessary for the anatomical and functional development of the visual system.**

In the visual system of mammals, the projections of retinal ganglion cells (RGCs) from each eye are initially intermixed in their thalamic target, the dorso-lateral geniculate nucleus (dLGN), and subsequently segregate into eye-specific layers through an activity-dependent process (1–4). RGCs spontaneously fire periodic bursts of action potentials that sweep across the immature retina in a wave-like manner from embryonic age until eye opening, at the time retinogeniculate projections segregate (5–11). The mechanism of wave propagation is not fully understood. Yet, synaptic transmission mediated by nicotinic acetylcholine receptors (nAChRs) on RGCs appears to be necessary for the genesis of these waves and for the segregation process (12, 13).

Neuronal nAChRs are pentameric ligand-gated ion channels encoded by a large multigene family consisting of at least eight $\alpha$ ($\alpha 2$–9) and three $\beta$ ($\beta 2$–4) subunit genes (14–16). These subunits associate into functional homopentamers ($\alpha 7$, $\alpha 8$, or $\alpha 9$) or heteropentamers, most likely comprised of two $\alpha$ and three $\beta$ subunits.

In recent years, the availability of mutant mice lacking single nAChR subunits has circumvented the lack of subtype-specific agonists and antagonists and given new impetus to the study of nAChR physiology (17). These transgenic animals represent unique tools to study the role of nAChRs in complex circuits and the related functions or behaviors.

In particular, in the case of retinal development, it has been shown that mice lacking the $\beta 2$ subunit exhibit no correlated spontaneous activity in the retina during the first week of postnatal life, indicating that $\beta 2$ subunit-containing nAChRs are critical in establishing this phenotype (18). The aim of the present paper is to exploit the facilities offered by the animal model of $\beta 2-/-$ mice (19) to investigate the role of nAChRs in the development of the connectivity and related function of the visual system. In particular, we evaluate the hypothesis that the lack of spontaneous retinal activity in $\beta 2-/-$ mice causes abnormalities in the development of retinogeniculate connections. As the distribution of $\beta 2$ and $\alpha 4$ nAChR subunits largely overlaps in the brain and these subunits are thought to combine to form the predominant nAChR isoform in central neurons, we also study a strain of mutant mice lacking the $\alpha 4$ subunit (20). Moreover, we analyze possible functional counterparts of the anatomical defect by studying the extent of the binocular subfield of the visual cortex as well as the retinal and cortical visual acuity.

## Materials and Methods

**Animals.** The $\beta 2-/-$ and the $\alpha 4-/-$ mice (backcrossed for at least six generations to the C57BL6/6J parental strain), produced at the Pasteur Institute (Paris), have been described (19–21). $\beta 2-/-$ mice show abnormal passive avoidance behavior (19), increased neurodegeneration with aging (21), and, similar to $\alpha 4-/-$ mice, a reduced antinociceptive response to nicotine (20).

**Intraocular Injection.** All animals were used in accordance with the Centre National de la Recherche Scientifique guidelines for care and use of laboratory animals. Mice were anesthetized with a solution of 1.5% ketamine, 0.05% xylazine in PBS for adults (150 $\mu$l/30 g body weight) or with hypothermia for pups. A solution of 30–60% horseradish peroxidase (HRP, type VI; Sigma) in physiological solution containing 2% DMSO was injected into the vitreous chamber of the eye by using a glass needle inserted just behind the corneo-scleral margin of the eye. A total of 3–4 $\mu$l of HRP was injected into the eye of adult mice and 1–2 $\mu$l for pups. After 24 h, mice were anesthetized and perfused with 0.9% saline, followed by 1.25% glutaraldehyde, 1% paraformaldehyde in 0.1 M phosphate buffer, pH 7.4. Cryoprotected brains were cut on a freezing microtome into 40-$\mu$m coronal sections. A modified tetramethylbenzidine reaction was used for HRP-labeling revelation. One microliter of (±)Epibatidine-L-tartrate (1 mM in physiological solution; Research Biochemicals) was binocularly injected in mouse pups every 24 h starting at postnatal day 3 (P3). Care was taken to insert the needle in the same hole at each repeated injection.

**Determination of dLGN Fraction Occupied by Ipsilateral Projection.** HRP-labeled dLGN sections were examined under bright-field illumination. Images were acquired by using a charge-coupled device camera mounted on a Leica microscope, digitized by the VISION EXPLORER VA program (Graftek, Mirmande, France), and analyzed by using the National Institutes of Health IMAGE program. The limits of the ipsilateral and contralateral dLGN projections were either traced with the mouse on the computer screen or were obtained by setting an optical density threshold to include all

NEUROBIOLOGY

Abbreviations: RGC, retinal ganglion cell; dLGN, dorso-lateral geniculate nucleus; nAChR, nicotinic acetylcholine receptor; HRP, horseradish peroxidase; SC, superior colliculus; VEP, visual evoked potential; pERG, pattern electroretinogram; P*n*, postnatal day *n*.

§Present address: Department of Molecular and Human Genetics, Baylor College of Medicine, One Baylor Plaza, Houston, TX 77030.

¶To whom reprint requests should be addressed. E-mail: changeux@pasteur.fr.

The publication costs of this article were defrayed in part by page charge payment. This article must therefore be hereby marked "*advertisement*" in accordance with 18 U.S.C. §1734 solely to indicate this fact.

HRP-labeled elements (artifactual labeling, such as blood vessels, was interactively erased). Attention was taken to exclude the ventral LGN, intrageniculate leaf, and extrageniculate optic tract. For each brain, an internally controlled measure of the dLGN fractional area occupied by the ipsilateral projection was obtained by dividing the average of the four largest ipsilateral areas (corresponding to the middle third of the dLGN) by the average of the four largest total dLGN areas (assessed by the outer boundaries of the contralateral projection zones on the corresponding section).

**Electrophysiology.** Sixteen adult wild-type and $\beta2-/-$ mice were used. Anesthetized mice (urethane 20% in saline, 8 ml/kg, Sigma) were mounted in a stereotaxic apparatus. Body temperature was monitored with a rectal probe and maintained at 37°C with a heating pad. A large portion of the skull ($4 \times 4$ mm) overlying the binocular visual cortex of the right side was drilled and removed, leaving the dura intact. Using a computer-driven three-axis motorized manipulator, the recording electrode (a glass micropipette filled with 3 M NaCl, 1–2 M impedance) was inserted at 2.0 to 3.2 mm lateral to the lambda. Single units were recorded at 3.1 mm from lambda to check that their receptive field corresponded to the location of the vertical meridian. For visual evoked potential (VEP) recording, the microelectrode was advanced 100 $\mu$m within the cortex. Electrical signals were amplified (50,000 fold), band-pass filtered (0.3–100 Hz, $-6$ dB/oct), digitized (12-bit resolution), and averaged (at least 128 events in blocks of 16 events each) in synchrony with the stimulus contrast reversal. Transient VEPs in response to abrupt contrast reversal (1 Hz) of the grating stimuli were evaluated by measuring the peak-to-trough amplitude. Visual stimuli were horizontal sinusoidal gratings of different spatial frequency and contrast generated by a VSG2/2 card (Cambridge Research System, Cheshire, U.K.) and presented on the face of a monitor (Barco CCID 7751, Brussels, Belgium) suitably linearized by gamma correction. The display (mean luminance 25 cd/m$^2$, area $24 \times 26$ cm) was placed 14 cm in front of the animal and positioned laterally to the vertical midline, thereby covering $81 \times 86$ degrees of the left visual field (see Fig. 3*a*). For pattern electroretinogram (pERG) recording, the visual stimulus was centered on the projection of the pupil. Retinal signals were recorded by means of a small silver loop positioned with a micromanipulator in such a way as to encircle the pupil. The reference and ground electrodes were subdermal stainless steel needles positioned on the skull. Signals were amplified (100,000 fold), filtered (1–30 Hz), and averaged (at least 400 sweeps) in response to 1-Hz contrast-reversing gratings of high contrast (90%) and different spatial frequency (0.05–0.5 c/degrees). Under these conditions the pERG waveform consists of a positive-negative complex with a peak time of 90 and 180 ms, respectively, and a peak-to-trough amplitude of about 7 $\mu$V at 0.05 c/degrees.[‖] Retinal acuity was estimated with the same protocol used for cortical acuity (22).

## Results

**Altered Retinofugal Projections in Adult $\beta2-/-$ Mice.** To study the distribution of retinogeniculate projections, experimental animals were monocularly injected with the neuronal tracer HRP. In adult wild-type mice the majority of retinogeniculate projections cross at the level of the optic chiasm to terminate in the contralateral dLGN (23). The terminals of these fibers are unevenly distributed. Contralateral fibers innervate the "outer shell" of the nucleus, located caudo-dorsally, and leave a gap in the dorso-medial part, corresponding to the "inner core," that receives afferents exclusively from the ipsilateral retina. The uncrossed fibers originating from the ipsilateral retina present the complementary pattern of labeling (Fig. 1*a*). In $\beta2-/-$ adult mice (>60 postnatal days), the spatial distribution of retinogeniculate terminals was strikingly different. The contralateral projection to the dLGN occupied the whole nucleus and completely invaded the territory occupied by ipsilateral axons in the wild type. The ipsilateral fibers remained confined to the dorso-medial aspect of the nucleus but spread largely into the territory normally occupied by the contralateral projection (Fig. 1*b*). Thus, the deletion of the $\beta2$ subunit of nAChRs resulted in a strong impairment of the normal distribution of retinogeniculate projections.

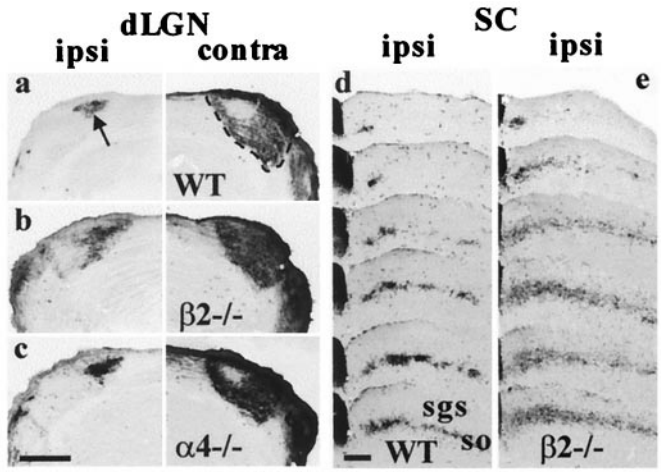


**Fig. 1.** HRP labeling of retinogeniculate (*a–c*) and retinocollicular (*d* and *e*) projections in adult mice. (*a–c*) Representative coronal sections of dLGNs in adult wild-type (WT) (*a*), $\beta2-/-$ (*b*), and $\alpha4-/-$ (*c*) mice. Note the abnormal segregation of retinogeniculate afferents in $\beta2-/-$ mice (dashed lines represent the borders of the dLGN; the arrow indicates the labeled area from the ipsilateral eye). (*d* and *e*) Representative rostro-caudal (from bottom to top) series of one in four coronal sections through the ipsilateral SC of adult wild-type (*d*) and $\beta2-/-$ (*e*) mice. Note the abnormal distribution of ipsilateral afferents in $\beta2-/-$ mice. ipsi = ipsilateral; contra = contralateral; so = stratum opticum; sgs = stratum griseum superficiale. [Scale bar (*a-c*) 350 $\mu$m; (*d* and *e*) 200 $\mu$m.]

As the $\alpha4\beta2$ subtype constitutes the vast majority of nAChRs in the brain, the retinogeniculate pattern of labeling was analyzed on another strain of transgenic mice that lack the $\alpha4$ subunit of nAChRs. In contrast to the results observed in $\beta2-/-$ mice, we found that in $\alpha4-/-$ adult mice the pattern of retinogeniculate labeling did not significantly differ from that of wild-type mice, indicating that the $\alpha4$ subunit was not required for the determination of the adult organization of retinal afferents in the dLGN (Fig. 1*c*).

We also evaluated the pattern of retinofugal projections in another target of RGC axons, the superior colliculus (SC) (Fig. 1 *d* and *e*). In this nucleus, eye-specific areas also emerge from a process of activity-dependent segregation of crossed and uncrossed RGC projections (24–26). In adult wild-type mice, axons arising in the contralateral eye provide the principal input to the upper layers of the SC, the stratum opticum (SO), and the stratum griseum superficiale (SGS). The ipsilateral retinal projection is restricted mainly to the rostral part of the SC where it terminates principally in the SO. The distribution of ipsilateral fibers varies markedly along the rostro-caudal axis: rostrally, they form a series of patches distributed medio-laterally that concentrate as a single patch in the more caudal part of the SC (Fig. 1*d*). In the SC of adult $\beta2-/-$ mice the pattern of labeling of ipsilateral terminals differed considerably from wild-type mice. Their territory of innervation along the rostro-caudal axis of the SC was more extended than in wild-type mice. Both the SO and the SGS were densely innervated and, instead of the typical series of medio-lateral clusters, ipsilateral fibers formed a con-

[‖] Porciatti, V. & Falsini, B. (2000) *Invest. Ophthalmol. Visual Sci.* **41,** S500 (abstr.).

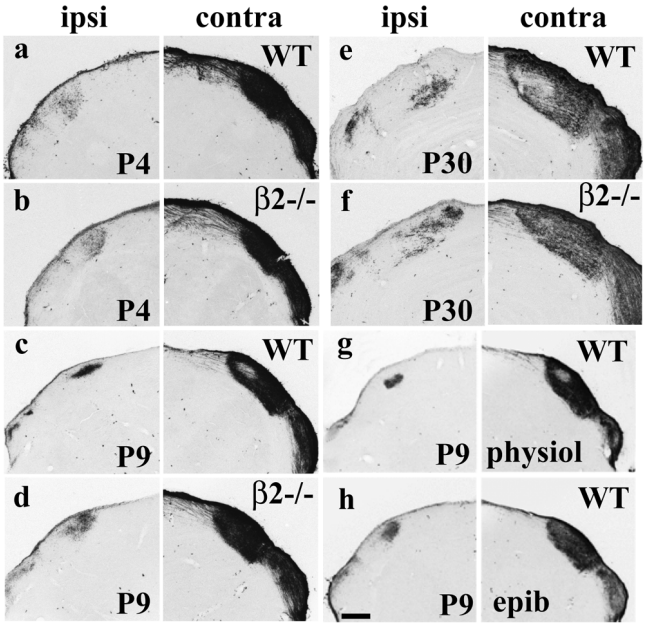


**Fig. 2.** HRP labeling of retinogeniculate projections in wild-type (WT) (*a, c,* and *e*) and $\beta2-/-$ (*b, d,* and *f*) mice at different postnatal ages during development (*a* and *b*: P4; *c* and *d*: P9; *e* and *f*: P30), and in normal mice binocularly injected with physiological solution (*g*) or epibatidine (*h*) from P3 to P7 and analyzed at P9. Note that in $\beta2-/-$ mice retinogeniculate segregation is normal at P4, but altered at P9 and P30. Abnormal segregation is also evident in mice treated with epibatidine (epib.) but not with physiological solution (physiol.). ipsi = ipsilateral; contra = contralateral. (Scale bar: 200 $\mu$m.)

tinuous band (Fig. 1*e*). No significant alterations could be observed in the distribution of the contralateral projection, because of the heavy and homogenously distributed labeling (data not shown). Consistent with the normal distribution of retinal terminals observed in the dLGN, adult mice lacking the $\alpha4$ subunit of nAChRs exhibited no defect at the level of the SC (data not shown).

**Development of the Retinogeniculate Projections in $\beta2-/-$ Mice.** To identify the stage of development at which the defects observed in $\beta2-/-$ mice occur, we examined the pattern of retinogeniculate labeling in wild-type and $\beta2-/-$ mice at different ages after birth. In wild-type mice, at P4 retinal fibers arising from the two eyes start to segregate, but are still largely intermixed with each other. The contralateral projection occupies the entire dLGN, and the ipsilateral projection is diffusely distributed on a large part of the nucleus (Fig. 2*a*). At P9 the process of segregation is almost accomplished and eye-specific layers are easily detected (Fig. 2*c*). At P30 the distribution of retinogeniculate projections is adult-like: crossed fibers terminate in the ''outer shell'' and ipsilateral fibers in the ''inner core'' (Fig. 2*e*). The developmental analysis of $\beta2-/-$ mice did not reveal significant differences in the distribution of retinogeniculate projections at P4, compared with wild-type mice (Fig. 2*b*). Yet, in $\beta2-/-$ mice, at P9 retinal projections, instead of segregating, remained intermixed. The contralateral projection still occupied the whole dLGN and the ipsilateral projection was diffusely distributed in the dorsomedial part of the nucleus (Fig. 2*d*). A similar alteration in the distribution of retinogeniculate fibers was observed in $\beta2-/-$ mice at P30 (Fig. 2*f*). The alteration in retinogeniculate projections is better appreciated by analyzing the size of the ipsilateral retinal projection to the dLGN. Quantitative measurements, obtained by computerized image analysis of the fraction of the dLGN occupied by the ipsilateral projection, confirmed that the difference between $\beta2-/-$ and wild-type mice is present at P9 and at P30 but not at P4 (Table 1).

**Table 1. Percentage of dLGN area occupied by ipsilateral fibers**

| | P4 | P9 | P30 |
|---|---|---|---|
| WT | 46.0 ± 0.5 | 19.2 ± 0.4 | 16.6 ± 0.3 |
| $\beta2-/-$ | 45.6 ± 0.2 | 39.6 ± 1.0* | 34.0 ± 1.3* |
| Physiol. | | 18.3 ± 0.6 | |
| Epib. | | 40.0 ± 0.9*† | |

Percentage of dLGN area occupied by ipsilateral fibers in wild-type (WT) and $\beta2-/-$ mice at different postnatal ages, and in WT mice binocularly injected with 1 mM epibatidine (epib.) or physiological solution (physiol.) from P3 to P7 and analyzed at P9. Mean values ± SEM are shown. P4 (WT, $n$ = 8; $\beta2-/-$, $n$ = 6); P9 (WT, $n$ = 6; $\beta2-/-$, $n$ = 12; epib., $n$ = 6; physiol., $n$ = 6); P30 (WT, $n$ = 10; $\beta2-/-$, $n$ = 8). Statistical analysis according to one-way ANOVA followed by post hoc Fischer test for multiple comparisons (limited to P9): *, $P < 0.0001$ vs. WT; †, $P < 0.0001$ vs. physiol.

**Pharmacologically Elicited Alteration of Retinogeniculate Projections.** Previous results, obtained in the ferret, showed that epibatidine, a potent nAChR agonist, is a good candidate for *in vivo* prolonged blockade of retinal nAChRs. In fact, at 1 nM concentration, epibatidine blocks *in vitro* the generation of retinal waves through receptor desensitization, and, when given intraocularly, affects the retinogeniculate segregation (13, 27–29). We used a similar experimental protocol to verify whether epibatidine also can impair the segregation process in the mouse visual pathway. Moreover, we compared the effects of a pharmacological blockade of retinal nAChRs on retinogeniculate segregation to those obtained after genetic deletion of the $\beta2$ subunit of nAChRs. Epibatidine (1 $\mu$l/eye, 1 mM in physiological solution) was binocularly injected in wild-type mice every 24 h from P3 to P7, which is the critical period of retinogeniculate segregation, to provide a prolonged inhibition of nAChRs at the retinal level. Mice were monocularly injected with HRP at P8 and the pattern of RGC axons labeling in the dLGN was observed in coronal sections. The segregation of eye inputs, from an initially intermixed state, occurred normally between P4 and P9 in animals that received repeated injections of control physiological solution (Fig. 2*g*). In contrast, the pattern of ocular inputs was substantially altered in mice repeatedly treated with epibatidine. The contralateral projection occupied the entire extent of the dLGN and no gap in the dorso-medial part was detected. Ipsilaterally, retinal fibers were distributed in the dorso-medial aspect of the nucleus but were more diffuse than in control mice (Fig. 2*h*). Quantitative measurements confirmed that the fraction of the dLGN occupied by the ipsilateral projection was significantly larger in epibatidine-treated mice than in controls and was comparable to that observed in $\beta2-/-$ mice of the same age (Table 1).

**Functional Expansion of the Binocular Visual Cortex in $\beta2-/-$ Mice.** We analyzed possible consequences of the $\beta2$ subunit deletion on the visual cortical topography by using a physiological approach. We evaluated the extension of the binocular area (area Oc1b) of the primary visual cortex in adult $\beta2-/-$ and wild-type mice by recording VEPs from a series of locations across the medio-lateral extent of the cortex, in response to stimulation of either eye. The Oc1b area, where responses from both eyes can be recorded, is bordered laterally by the secondary visual area (Oc2) and medially by the monocular area of the primary visual cortex (area Oc1m), which receives visual inputs exclusively from the contralateral eye (Fig. 3*a*). The amplitude of VEPs after stimulation of the ipsilateral eye was maximal at 3.1 mm from lambda, the site at which the vertical meridian is

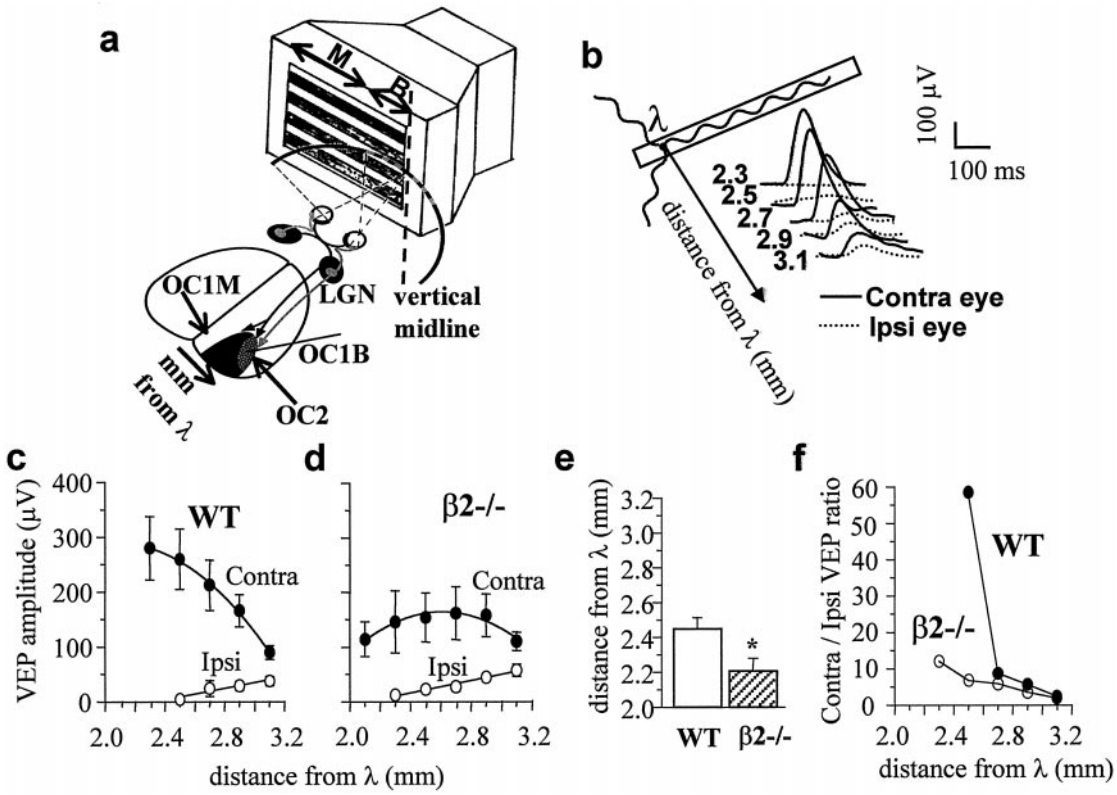


**Fig. 3.** (*a*) Sketch of the mouse visual system and stimulating apparatus. The visual field is divided in a smaller, central zone that can be seen by both eyes (binocular, B) and a larger, lateral zone that can be seen by the one eye only (monocular, M). The primary visual cortex, which contains the representation of the contrateral hemifield, is divided in a smaller, lateral area receiving the input of both eyes (OC1b), and a larger, medial area receiving the input of the contralateral eye only (OC1m). The stimulus consisted of a computer generated grating presented to the contralateral visual field. (*b*) Representative examples of VEP responses to stimulation of the ipsilateral and the contralateral eye, recorded from different locations of the binocular portion of the primary visual cortex (Oc1b). When the recording electrode is moved medially, the response of the ipsilateral eye tends to vanish whereas the response of the contralateral eye increases. (*c* and *d*) Representative medio-lateral cortical profile of VEP amplitude for the contralateral and the ipsilateral eye in a wild-type (WT) (*c*) and a $\beta2-/-$ (*d*) mouse. The response of the ipsilateral eye is recordable at more medial cortical locations in $\beta2-/-$ mice than in wild-type mice. For the contralateral eye responses in the Oc1m (at 2.3 mm for WT and 2.1 mm for $\beta2-/-$) are reported. (*e*) The medial border of the Oc1b area (obtained by extrapolating to 0 V the medio-lateral profile of the VEP amplitude) was significantly more medial in $\beta2-/-$ mice ($2.21 \pm 0.05$, $n = 5$) than in wild type ($2.46 \pm 0.06$, $n = 4$). Bars represent mean ± SEM. *, $P < 0.05$, Student's *t* test. (*f*) Representative medio-lateral profile of the amplitude ratio between contralaterally and ipsilaterally driven responses. Ratios were evaluated from average amplitude data represented in *c* and *d*. In the wild-type mouse, when the recording electrode moves medially, the contralateral/ipsilateral VEP ratio increases dramatically, whereas in the $\beta2-/-$ mouse it is less steep. In the range 3.1 to 2.7 mm from lambda, the slope of the VEP ratio is approximately linear for both wild-type and $\beta2-/-$ mice. The average difference in the slope, evaluated from linear regression lines of individual mice, is statistically significant ($\beta2-/-$, $n = 5$; wild type, $n = 4$; $P < 0.05$, Student's *t* test).

represented and which delimitates the lateral border of the Oc1b area. When the recording microelectrode was progressively moved to more medial locations (toward the lambdoid scissure), the VEPs of the ipsilateral eye progressively decreased in amplitude, vanishing in wild-type mice at about 2.5 mm from lambda ($2.46 \pm 0.06$ mm), a location corresponding to the medial border between the monocular and the binocular area. The VEPs of the contralateral eye showed the opposite behavior. Their amplitude was minimal at the level of the vertical meridian (3.1 mm from lambda) and tended to increase when the recording microelectrode was moved medially (Fig. 3 *b* and *c*). In $\beta2-/-$ mice, VEP responses to stimulation of the ipsilateral eye were recorded up to 2.2 mm from lambda ($2.21 \pm 0.05$ mm) (Fig. 3*d*). Mean values are represented in Fig. 3*e*. Thus, responses of the binocular area were recorded in adult wild-type mice for ≈0.64 mm along the medio-lateral extent of the primary visual cortex, and in $\beta2-/-$ mice for ≈0.89 mm, indicating about 39% increase in the extension of the binocular area in $\beta2-/-$ mice with respect to wild type.

At all locations in the Oc1b area, the VEPs of the contralateral eye were larger than those of the ipsilateral eye, in both wild-type and $\beta2-/-$ mice (Fig. 3 *c* and *d*). The VEP amplitude ratio between the contralateral and the ipsilateral eye (contra/ipsi VEP ratio) represents an index of the relative strength of either eye in driving cortical responses (30, 31). The contra/ipsi VEP ratio is close to two at 3.1 mm from lambda (location of the vertical meridian) and increases dramatically for more medial locations, revealing a steep physiological transition between the binocular and the monocular visual cortex. We found that in adult $\beta2-/-$ mice the slope of the contra/ipsi VEP ratio across binocular cortical locations was less steep than in wild type, indicating a smooth transition from the binocular to the monocular visual cortex in the $\beta2-/-$ mice compared with wild type (Fig. 3*f*).

**Reduced Visual Acuity in $\beta2-/-$ Mice.** To analyze possible consequences of the lack of the $\beta2$ subunit gene on visual function, we measured VEP visual acuity, a well-established measure of overall visual function in mammals (32–35). VEP responses to alternating gratings decrease in amplitude in response to increases in the spatial frequency of the stimulus (see legend Fig. 4). In adult $\beta2-/-$ mice visual acuity was found to be reduced by a factor of 2 compared with wild-type mice ($0.59 \pm 0.08$ c/degrees; $\beta2-/-$, $0.30 \pm 0.05$ c/degrees) (Fig. 4*a* and mean

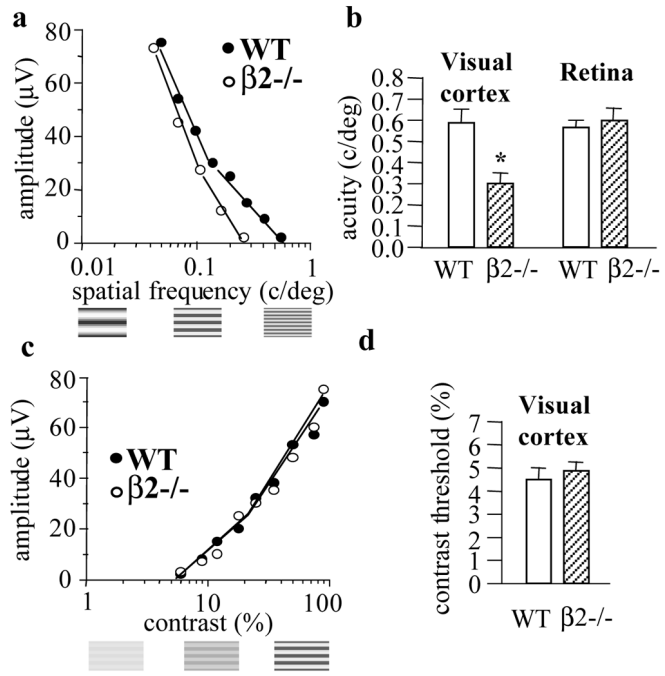


**Fig. 4.** (*a*) Representative examples of VEP amplitude changes in response to gratings of high contrast and of decreasing bar size (increasing spatial frequency) in a wild-type (WT) and a $\beta2-/-$ mouse. VEP amplitude decreases by progressively increasing the spatial frequency. Visual acuity was determined by linearly extrapolating VEP amplitude to 0 V, the set of data points close to the noise level. Examples of gratings of increasing spatial frequency are shown below the abscissae. (*b*) Spatial resolution in the visual cortex and in the retina of wild-type and $\beta2-/-$ mice. Visual acuity is significantly reduced in $\beta2-/-$ mice compared with wild-type mice at the cortical ($\beta2-/-$, 0.30 ± 0.05 c/degrees, $n = 9$; WT, 0.59 ± 0.08 c/degrees, $n = 4$; *, $P < 0.01$, Student's *t* test) but not at the retinal level ($\beta2-/-$, 0.60 ± 0.07 c/degrees, $n = 3$; WT, 0.57 ± 0.04 c/degrees, $n = 3$; $P > 0.05$, Student's *t* test). Bars represent mean ± SEM. (*c*) Representative examples of VEP amplitude changes in response to coarse gratings (0.06 c/degrees) of decreasing contrast. VEP amplitude decreases by progressively reducing the contrast. Contrast threshold was determined by linear extrapolation of VEP amplitude to 0 V, the set of data points close to the noise level. Examples of gratings of increasing contrast are shown below the abscissae. (*d*) Contrast threshold is normal in $\beta2-/-$ mice compared with wild type ($\beta2-/-$, 4.8 ± 0.3%, $n = 4$; WT, 4.6 ± 0.5%, $n = 3$; $P > 0.05$, Student's *t* test). Bars represent mean ± SEM.

values in Fig. 4*b*). This reduction was not due to alterations in optical factors, such as optical opacities or defocus. In fact, contrast threshold, which is known to be strongly impaired by optical alterations (36), was not affected by the absence of the $\beta2$ subunit (wild type, 4.6 ± 0.5%; $\beta2-/-$, 4.8 ± 0.3%) (Fig. 4*c* and mean values in Fig. 4*d*).

The low visual acuity of adult $\beta2-/-$ mice, observed by recording VEPs from the cortex, could potentially originate from alterations occurring along postretinal pathways or result from defects present within the retina. To distinguish between these two possibilities, we evaluated spatial resolution at the retinal level by recording the pERG in response to alternating gratings of various spatial frequencies (22). The highest spatial frequency able to evoke a pERG response represents an index of the resolution of the retinal output (pERG acuity) (22, 37, 38). In adult wild-type mice, the pERG acuity closely matched that measured at the cortical level (0.57 ± 0.04 c/degrees). We found that in adult $\beta2-/-$ mice the spatial resolution at the retinal level was normal compared with wild-type mice (0.60 ± 0.07 c/degrees) (Fig. 4*b*). Therefore, the functional deficits observed at the level of the visual cortex in adult $\beta2-/-$ were not due to defects present within the adult retina, but resulted from a developmental alteration along the postretinal pathways.

## Discussion

Pharmacological studies suggest that nAChR-dependent retinal waves of spontaneous activity regulate the process of segregation of retinogeniculate projections in the course of postnatal development (13). Yet, the techniques commonly used to elicit a long-lasting blockade of retinal activity *in vivo* in young animals may nonspecifically affect visual development. In particular, the concentration and specificity of pharmacological compounds given *in vivo* are difficult to assess. In addition, no subtype-specific agonists or antagonists for nAChRs are available. To obviate these difficulties and to ascertain the role played by specific nAChR subunits in the anatomical and physiological development of the visual system, we used genetically modified mice lacking a particular nAChR subunit (17, 19, 20).

In $\beta2-/-$ mice, the pattern of retinogeniculate and retinocollicular projections was found to be altered. In contrast, although the $\alpha4$ subunit is the predominant partner of the $\beta2$ subunit in the formation of brain nAChRs, its deletion did not cause defects in retinofugal segregation. These results indicate that the $\beta2$ subunit of nAChRs, but not the $\alpha4$ subunit, is necessary for the process of segregation.

The initial developmental phase of retinal projections looked normal in $\beta2-/-$ mice until P4. This result, together with previous observations showing that the anatomy (18) and the spatial resolution of the retina (this paper) were normal in $\beta2-/-$ mice, indicate that the deficit observed at later ages is not due to defects in RGC-programmed cell death or pathfinding errors of retinal fibers, but to the aberrant segregation of ipsilateral and contralateral fibers at the target level.

The extent of the alteration in the distribution of retinogeniculate fibers observed in $\beta2-/-$ mice at P9 was similar to that observed after intraocular epibatidine-elicited blockade of retinal nAChRs from P3 to P8. This result suggests that the first 10 days of postnatal life constitute a critical period during which activation of $\beta2$ subunit-containing nAChRs of retinal origin is required for segregation.

How does the genetic deletion of the $\beta2$ gene cause the observed anatomical defect in the distribution of retinofugal projections? After the observation that $\beta2-/-$ mice exhibit no correlated spontaneous activity in the retina (18), the most likely explanation is that the defect of retinofugal segregation observed in $\beta2-/-$ mice results from the absence of spontaneous retinal activity. Thus, by entering the composition of the nAChR oligomer(s) necessary for wave generation at a critical moment during development, the $\beta2$ subunit would play a fundamental role in shaping the adult organization of topographical maps in the visual pathways.

The existence of multiple nAChR subunits and oligomers in the brain and retina makes it difficult to identify the nAChR isoform(s) responsible for retinal waves and visual development. By using genetically modified mice, we showed that the $\beta2$ subunit, but not the $\alpha4$ subunit, is necessary for the anatomical development of the visual system. The analysis of retinal waves in mice lacking single nAChR subunits indicated that the $\beta2$ subunit, but not the $\alpha3$ subunit, is required to form nAChRs that mediate cholinergic waves; pharmacological evidence excluded the participation of the homopentameric $\alpha7$-containing nAChRs (18). Altogether these findings suggest that the nAChR subtype involved in this process contains the $\beta2$ subunit but that the $\alpha3$ and the $\alpha7$ subunits are not necessary. Moreover, in contrast to what has been observed in the central nervous system, the $\alpha4$ subunit is not likely to be the preferred partner of the $\beta2$ subunit at the retinal level. Other possible candidates for the assembly in the retina of the relevant nAChR(s) are the $\alpha2$, $\alpha5$, or $\alpha6$

subunits, which, together with $\beta 2$, $\beta 3$, and $\beta 4$ subunits, are expressed in the retina (39–41).

The genetic deletion of the $\beta 2$ subunit of nAChRs resulted in anatomical as well as physiological deficits. $\beta 2-/-$ mice showed binocular responses even at cortical locations normally responsive only to the contralateral eye, indicating a functional expansion of the binocular visual cortex. This effect is consistent with the anatomical data showing an altered segregation of retinogeniculate fibers. Indeed, the altered segregation resulted in an enlarged ipsilaterally driven dLGN subfield that activated a larger cortical area.

Visual acuity is a reliable measure of the overall visual function and was found to be significantly decreased in adult $\beta 2-/-$ mice at the cortical level. The low visual acuity did not result from deficits present in the adult retina, because the retinal output was shown to have normal spatial resolution. In addition, this result indicates that the $\beta 2$ subunit of the nAChRs is not required for the functioning of the adult retina. As the size of receptive fields is known to strictly correlate with visual acuity (34), the $\beta 2-/-$ phenotype can be most likely interpreted on the basis of abnormally large receptive fields resulting from alterations in the segregation process during development.

These data are consistent with the notion that a single genetic event, which eliminates a neurotransmitter receptor at the peripheral level, here the $\beta 2$ subunit-containing nAChR in the retina, alters a spontaneous retinal activity that is required during postnatal development for the epigenetic (42) maturation of the central visual system at both the anatomical and the functional level.

We thank Nicolas Champtiaux, Didier de Saint Jan, Patricia Gaspar, Martine Usdin, and Michele Zoli for useful comments and discussion on the manuscript and Carlo Orsini and Elena Putignano for technical help. This work was supported by Collège de France, Centre National de la Recherche Scientifique, Association Française contre les Myopathies, Commission of the European Communities (CEC), Association pour la Recherche sur le Cancer (ARC), Ministero dell'Universitá e della Ricerca Scientifica e Tecnologica Cofinanziamento 2000/2001, Consiglio Nazionale delle Ricerche-targeted project in Biotechnology SP-5, Progetto Strategico Neuroscienze and Progetto Telethon 934 and E833. F.M.R. is supported by an European Molecular Biology Organization fellowship (ALTF457).

1. Shatz, C. J. & Stryker, M. P. (1988) *Science* **242,** 87–89.
2. Sretavan, D. W., Shatz, C. J. & Stryker, M. P. (1988) *Nature (London)* **336,** 468–471.
3. Hahm, J.-O., Langdon, R. B. & Sur, M. (1991) *Nature (London)* **351,** 568–570.
4. Katz, L. C. & Shatz, C. J. (1996) *Science* **274,** 1133–1138.
5. Galli, L. & Maffei, L. (1988) *Science* **242,** 90–91.
6. Maffei, L. & Galli-Resta, L. (1990) *Proc. Natl. Acad. Sci. USA* **87,** 2861–2864.
7. Meister, M., Wong, R. O., Baylor, D. A. & Shatz, C. J. (1991) *Science* **252,** 939–943.
8. Wong, R. O. L., Meister, M. & Shatz, C. J. (1993) *Neuron* **11,** 923–938.
9. Mooney, R., Penn, A. A., Gallego, R. & Shatz, C. J. (1996) *Neuron* **17,** 863–874.
10. Wong, R. O. L. (1999) *Annu. Rev. Neurosci.* **22,** 29–47.
11. Roerig, B. & Feller, M. B. (2000) *Brain Res. Rev*. **32,** 86–114.
12. Feller, M. B., Wellis, D. P., Stellwagen, D., Werblin, F. S. & Shatz, C. J. (1996) *Science* **272,** 1182–1187.
13. Penn, A. A., Riquelme, P. A., Feller, M. B. & Shatz, C. J. (1998) *Science* **279,** 2108–2112.
14. Sargent, P. B. (1993) *Annu. Rev. Neurosci.* **16,** 403–443.
15. Role, L. W. & Berg, D. K. (1996) *Neuron* **16,** 1077–1085.
16. Marubio, L. M. & Changeux, J.-P. (2000) *Eur. J. Pharmacol.* **393,** 113–121.
17. Cordero-Erausquin, M., Klink, R., Marubio, L. M. & Changeux, J.-P. (2000) *Trends Pharmacol. Sci.* **21,** 211–217.
18. Bansal, A., Singer, J. H., Hwang, B. J., Xu, W., Beaudet, A. & Feller, M. B. (2000) *J. Neurosci.* **20,** 7672–7681.
19. Picciotto, M. R., Zoli, M., Léna, C., Bessis, A., Lallemand, Y., LeNovère, N., Vincent, P., Merlo Pich, E., Brûlet, P. & Changeux, J.-P. (1995) *Nature (London)* **374,** 65–67.
20. Marubio, L. M., Arroyo-Jimenez, M. M., Cordero-Erausquin, M., Léna, C., Le Novère, N., de Kerchove d'Exaerde, A., Huchet, M., Damaj, M. I. & Changeux, J.-P. (1999) *Nature (London)* **398,** 805–810.
21. Zoli, M., Picciotto, M. R., Ferrari, R., Cocchi, D. & Changeux, J.-P. (1999) *EMBO J.* **18,** 1235–1244.
22. Porciatti, V., Pizzorusso, T., Cenni, M. C. & Maffei, L. (1996) *Proc. Natl. Acad. Sci. USA* **93,** 14955–14959.
23. Godement, P., Salaün, J. & Imbert, M. (1984) *J. Comp. Neurol.* **230,** 552–575.
24. Fawcett, J. W., O'Leary, D. D. M. & Cowan, W. M. (1984) *Proc. Natl. Acad. Sci. USA* **81,** 5589–5593.
25. O'Leary, D. M., Fawcett, J. W. & Cowan, W. M. (1986) *J. Neurosci*. **6,** 3692–3705.
26. Thompson, I. & Holt, C. (1989) *J. Comp. Neurol.* **282,** 371–388.
27. Badio, B. & Dali, J. W. (1994) *Mol. Pharmacol.* **45,** 563–569.
28. Kittila, C. A. & Massey, S. C. (1997) *J. Neurophysiol.* **77,** 675–689.
29. Marks, M. J., Robinson, S. F. & Collins, A. C. (1996) *J. Pharmacol. Exp. Ther*. **277,** 1383–1396.
30. Porciatti, V., Pizzorusso, T. & Maffei, L. (1999) *Vision Res.* **39,** 3071–3081.
31. Huang, Z. J., Kirkwood, A., Pizzorusso, T., Porciatti, V., Morales, B., Bear, M. F., Maffei, L. & Tonegawa, S. (1999) *Cell* **98,** 739–755.
32. Mohn, G. & Van Hof-van Duin, J. (1991) in *Vision and Visual Dysfunction*, ed. Regan, D. (Macmillan, London), pp. 179–211.
33. Birch, D. J. G. (1979) *Vision Res*. **19,** 933–937.
34. Fagiolini, M., Pizzorusso, T., Berardi, N., Domenici, L. & Maffei, L. (1994) *Vision Res.* **34,** 709–720.
35. Gianfranceschi, L., Fiorentini, A. & Maffei, L. (1999) *Vision Res.* **39,** 569–574.
36. Campbell, F. W. & Green, D. C. (1965) *J. Physiol. (London)* **181,** 576–593.
37. Fiorentini, A., Pirchio, M. & Sandini, G. (1984) *Hum. Neurobiol.* **3,** 93–95.
38. Ver Hoeve, J. N., Danilov, Y. P., Kim, C. B. & Spear, P. D. (1999) *Vis. Neurosci.* **16,** 607–617.
39. Hoover, F. & Goldman, D. (1992) *Exp. Eye Res*. **54,** 561–565.
40. Zoli, M., Le Novère, N., Hill, J. A., Jr., & Changeux, J.-P. (1995) *J. Neurosci.* **15,** 1912–1939.
41. Vailati, S., Hanke, W., Bejan, A., Barabino, B., Longhi, R., Balestra, B., Moretti, M., Clementi, F. & Gotti, C. (1999) *Mol. Pharmacol*. **56,** 11–19.
42. Changeux, J.-P. & Danchin, A. (1976) *Nature (London)* **264,** 23–30.